THE ASTROPHYSICAL JOURNAL SUPPLEMENT SERIES, 132:365–375, 2001 February

IN-ORBIT PERFORMANCE OF THE SPACE TELESCOPE NINA AND GALACTIC COSMIC-RAY FLUX MEASUREMENTS

V. BIDOLI, A. CANESTRO, M. CASOLINO, M. P. DE PASCALE, G. FURANO, A. IANNUCCI, A. MORSELLI, P. PICOZZA, E. REALI, AND R. SPARVOLI[1]
University of Rome "Tor Vergata" and INFN Section of Roma2, Via della Ricerca Scientifica 1, I-00133 Rome, Italy

A. BAKALDIN, A. GALPER, S. KOLDASHOV, M. KOROTKOV, A. LEONOV, V. MIKHAILOV, A. MURASHOV, AND S. VORONOV
Moscow Engineering Physics Institute, Kashirskoe Shosse 31, 115409 Moscow, Russia

M. BOEZIO, V. BONVICINI, R. CIRAMI, A. VACCHI, AND N. ZAMPA
University of Trieste and INFN Section of Trieste, Via A. Valerio 2, I-34147 Trieste, Italy

M. AMBRIOLA, R. BELLOTTI, F. CAFAGNA, F. CIACIO, M. CIRCELLA, AND C. DE MARZO
University of Bari and INFN Section of Bari, Via Amendola 173, I-70126 Bari, Italy

O. ADRIANI, P. PAPINI, S. PICCARDI, P. SPILLANTINI, AND S. STRAULINO
University of Florence and INFN Section of Florence, Largo Enrico Fermi 2, I-50125 Florence, Italy

S. BARTALUCCI, G. MAZZENGA, AND M. RICCI
INFN Laboratori Nazionali di Frascati, Via Enrico Fermi 40, I-00044 Frascati, Italy

AND

G. CASTELLINI
Istituto di Ricerca Onde Elettromagnetiche CNR, Via Panciatichi 64, I-50127 Florence, Italy
Received 2000 March 17; accepted 2000 September 28

ABSTRACT

The NINA apparatus, on board the Russian satellite *Resurs-01 No. 4*, has been in polar orbit since 1998 July 10, at an altitude of 840 km. Its main scientific task is to study the Galactic, solar, and anomalous components of cosmic rays in the energy interval 10–200 MeV nucleon^{-1}. In this paper we present a description of the instrument and its basic operating modes. Measurements of Galactic cosmic-ray spectra will also be shown.

Subject headings: cosmic rays — space vehicles

1. INTRODUCTION

With the launch of the telescope NINA on 1998 July 10, a wide program of satellite cosmic-ray observations began. The program aims to study the cosmic-ray radiation in a broad energy spectrum (from 10 to 10^5 MeV nucleon^{-1}) using a serious of dedicated satellite missions.

NINA (a New Instrument for Nuclear Analysis) has been developed by a joint program of the Italian National Institute of Nuclear Physics (INFN) and the Moscow State Engineering and Physics Institute (MEPhI). INFN consists of several Italian Institutes and Universities (WiZard group) who have carried out, together with European and American partners, balloon-borne experiments for the detection of cosmic antiparticles since 1989 (Golden et al. 1994, 1996; Hof et al. 1996; Barbiellini et al. 1996; Boezio et al. 1997, 1999; Basini et al. 1999; Boezio et al. 2000).

The link with the Russian counterpart was established in 1994, when the two sides started a collaboration and conceived the Russian-Italian Missions (RIM), of which NINA is the first step.

NINA's goal is to detect cosmic-ray nuclei of Galactic, solar, and anomalous origin, at 1 AU, from hydrogen to iron, between 10 and 200 MeV nucleon^{-1}. The experiment is carried out on board the satellite *Resurs-01 No. 4*, developed by the Russian space company VNIIEM. The spacecraft was launched into a polar Sun-synchronous orbit of altitude 840 km (Casolino et al. 1999a; Sparvoli et al. 2000).

NINA has been joined in space by a twin detector (NINA-2), placed again in a polar orbit but at a lower altitude (450 km). NINA-2 is housed on board the Italian satellite *MITA* (Casolino et al. 1999b), launched on 2000 July 15 from the Plesetsk launch facility in Russia by means of a Cosmos launcher. This second mission is intended to last for three years.

The RIM missions will then continue with the deployment of the PAMELA magnet spectrometer, which will be installed on board the satellite *Resurs-01 No. 5* and put in orbit at the beginning of the year 2003. The main objective of PAMELA is to perform high-precision measurements of antiparticle spectra (positrons and antiprotons) in the energy range from 0.1 GeV up to 200 GeV. In addition, it will measure electrons, protons, and the nuclear components of cosmic rays and will search for cosmic antinuclei (The PAMELA Collaboration 1999; Adriani et al. 1997).

This paper reports on the NINA mission, its scientific tasks, the organization of the detector with its ancillary instruments, the interface with the satellite, the launch phase, and finally the performance of the telescope in flight. In addition, it presents the reconstruction of the energy spectrum of the Galactic component of ^{4}He, ^{12}C, and ^{16}O in solar quiet conditions.

2. SCIENTIFIC OVERVIEW

NINA has been built in order to investigate the nuclear and isotopic composition of low-energy cosmic particles. Its low-altitude polar orbit (about 1.1 Earth radii) is particularly suitable for performing observations of particles of different origin while traversing regions of different geomagnetic cutoff. The Earth's magnetic field is utilized as a spectrometer. According to the coordinates along the orbit

[1] Sparvoli@roma2.infn.it.

where the particles are detected, it is possible to make inferences about their origin which can be Galactic, solar, or anomalous.

2.1. *Galactic Cosmic Rays*

Galactic cosmic rays (GCRs) are a directly accessible sample of matter coming from outside the solar system. The GCR energy spectrum can be well represented by a power-law energy distribution for energies above 1 GeV nucleon^{-1} but at lower energy shows a strong attenuation owing to the interaction between the solar wind and the cosmic particles (Wiedenbeck & Greiner 1980). This is one of the reasons why GCR investigations below 200 MeV nucleon^{-1} have been relatively scarce in the past.

NINA started its mission in a period of medium solar activity; the next solar maximum is foreseen for the year 2000. Owing to its technical characteristics and its good energy, mass, and angular resolution, the telescope is particularly suited for exploring the low-energy component of the cosmic radiation. The detector can record GCRs of very low energy (from 10 up to 200 MeV nucleon^{-1}) in the polar sectors of the orbit, where geomagnetic effects are virtually negligible.

2.2. *Solar Energetic Particles*

The most complete measurements of elemental abundances in the solar corona come from measurements of high-energy particles accelerated in the large solar energetic particle (SEP) events.

Initially it was thought that the energetic particles in large SEP events were accelerated in solar flares. In recent years, however, it has become clear that in the large *gradual* events particles are accelerated at shock waves that are driven out from the Sun by coronal mass ejections (CMEs) (Reames 1990, 1993, 1995; Gosling 1993; Reames 1998). These shocks accelerate the ions of the chemical elements in a fairly equivalent manner. In contrast, particles accelerated in *impulsive* solar flares show specific elemental enhancements produced by resonant wave-particle interactions during stochastic acceleration of the ions from the flare plasma.

New spacecraft observations can extend solar energetic particle measurements to heavier elements, to rarer elements, and to isotopes. NINA can perform SEP observations in the polar sectors of the orbit. Its good mass discrimination can help in the determination of their composition and therefore in the comprehension of the sources and acceleration mechanisms involved.

2.3. *Anomalous Cosmic Rays*

Anomalous cosmic rays (ACRs) are a low-energy component of interplanetary particles that include the elements H, He, C, N, O, and Ar (Klecker 1995; Simpson 1995). They are now known to originate from interstellar neutral particles that have been swept into the heliosphere, ionized by solar UV or charge exchange with the solar wind, convected into the outer heliosphere, and then accelerated to energies of $\sim$10 MeV nucleon^{-1} or more (Fisk, Kozlovsky, & Ramaty 1974). It is commonly assumed that the bulk of ACR acceleration takes place at the solar wind termination shock (Pesses, Jokipii, & Eichler 1981).

The observation of the anomalous N, O, and Ne ionic charge composition with the *SAMPEX* satellite (Baker et al. 1993) confirmed the theoretical predictions that ACRs are only partially charged; more precisely, singly charged ions dominate only at energies below $\sim$20 MeV nucleon^{-1} (Klecker et al. 1998), while at higher energies multiply charged ions become more abundant.

Being only partially ionized, ACRs have a much greater magnetic rigidity (at a given energy per nucleon) than either GCRs, which are essentially fully stripped, or SEPs, which have charge states characteristic of coronal temperatures. As a result, ACRs can be observed to much lower invariant latitude with a polar orbiting spacecraft like NINA.

3. THE NINA INSTRUMENT

NINA consists of the following four subsystems: (1) the *detector* (box *D*1), composed of 32 silicon layers and the electronics for signal processing; (2) the *on-board computer* (box *D*2), a dual microprocessor dedicated to data processing and to the selection of the trigger and the acquisition mode configuration; (3) the *interface computer* (box *E*), which rearranges the data coming from box *D*2 and delivers them to the satellite telemetry system; and (4) the *power supply* (box *P*), which distributes the power supply to the different subsystems.

The weight and electric power of the complete telescope are, respectively, 40 kg and 40 W, in accordance with the constraints imposed by the satellite. To safeguard from possible malfunctions and breaks, all electronic systems are global redundant.

The *detector* of NINA (box *D*1), manufactured by the Italian company Laben, is composed of 16 silicon planes. Every plane consists of a pair of *n*-type silicon detectors, 60×60 mm^2, each read out by 16 strips mounted back to back with orthogonal orientation, in order to measure the X and Y coordinates of the particle. The strip pitch is 3.6 mm.

The thickness of the first pair of detectors, composing the first plane of NINA, is 150 ± 15 μm; all the others, instead, are 380 ± 15 μm thick, for a total thickness of 11.7 mm of silicon in the whole detector. The indetermination in the total silicon thickness comes from the process of manufacturing and is greater (in percentage) for the first two thinner layers. In order to reduce to the minimum the thickness of dead area interposed between the silicon detectors, a special ceramic (Al_2O_3) frame, passing only under the lateral strips 1 and 16 and 625 μm thick, has been utilized. The role of the ceramic is to sustain the single silicon structures and connect them mechanically and electronically, by means of 64 pins, to the corresponding mother boards. A photo of the box *D*1 is shown in Figure 1.

Each plane of the detector with its electronics is mounted on an aluminum mother board. The 16 planes are vertically stacked (a sketch of the box *D*1 is visible in Fig. 2). The interplanar distance is 1.4 cm except for the first two planes, which are separated by 8.5 cm in order to improve the incident particles trajectory determination. They define the angular aperture of the telescope, which is about 32°. The 16 planes are modular, so that mechanically and electronically they are interchangeable. Below the 16 silicon planes, another four modules, dedicated to the trigger electronics, silicon power supply, analog-digital conversion, and FIFO, are placed.

The 20 plane structure is housed in a cylindrical aluminum vessel of 284 mm diameter and 480 mm height, filled up with nitrogen at 1.2 atm. The vessel is 2 mm thick, except for a window above the first silicon plane, where it is reduced to 300 μm (Fig. 2). The top part of the vessel is rounded, while

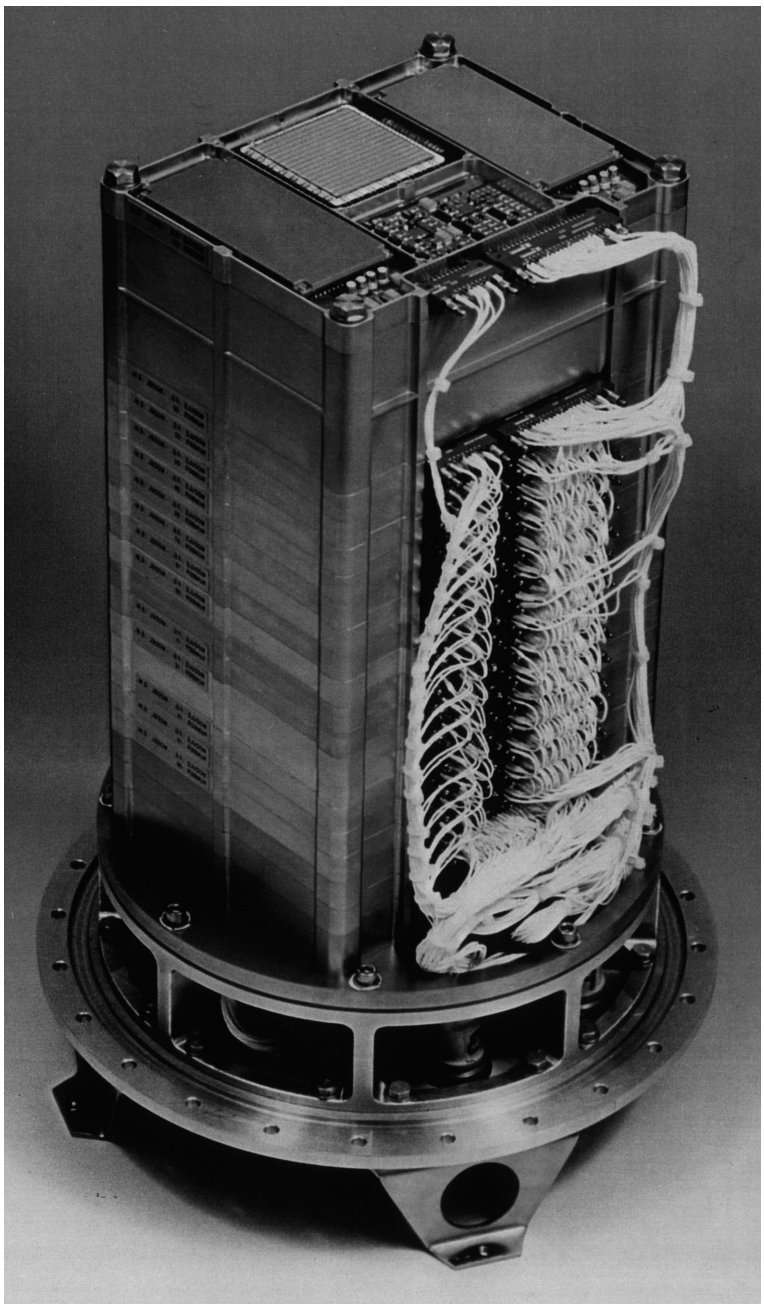

FIG. 1.—Photograph of the internal structure of box *D*1

the bottom part houses the connectors for the interfaces with the other parts of the detector.

The lateral strips (1 and16) of every silicon layer are used for the anticoincidence system (AC); they are read together by the same electronic channel, except for those of plane 1, where they are physically disconnected. A total number of 448 electronic channels, of the 512 available in the box *D*1, are used for the particle track and energy information; the anticoincidence system data occupy an additional 30 channels, while the remaining 34 are used for housekeeping data (16 plane currents, two temperatures, four voltages, one threshold level, 11 rate meters at different depths of the telescope), which monitor the status of the whole instrument.

The signals produced by the incoming particles in the silicon strips are first amplified and shaped. Every plane of the telescope has two 16 channels preamplifiers. Data are then converted to the digital format by means of a 12 bit ADC, with a full scale of 2800 mip (1 mip being equivalent to 30,400 electrons or about 105 keV of released energy). The resolution per channel is thus about 0.68 mip per channel, equivalent to 0.07 MeV per channel. There are two independent lines going to two different ADCs, for redundancy reasons. Only one is operating at a given moment. Before the ADC there are two gain amplifiers that can be selected depending on the acquisition mode: the first provides an amplification of a factor 32 (used only for noise tests) and the second of a factor 1 (active for normal acquisitions).

After conversion by ADC, data (1024 bytes per event) are sent through a FIFO to an eight-channel bus interface with the *on-board computer* (box *D*2), built again by the company

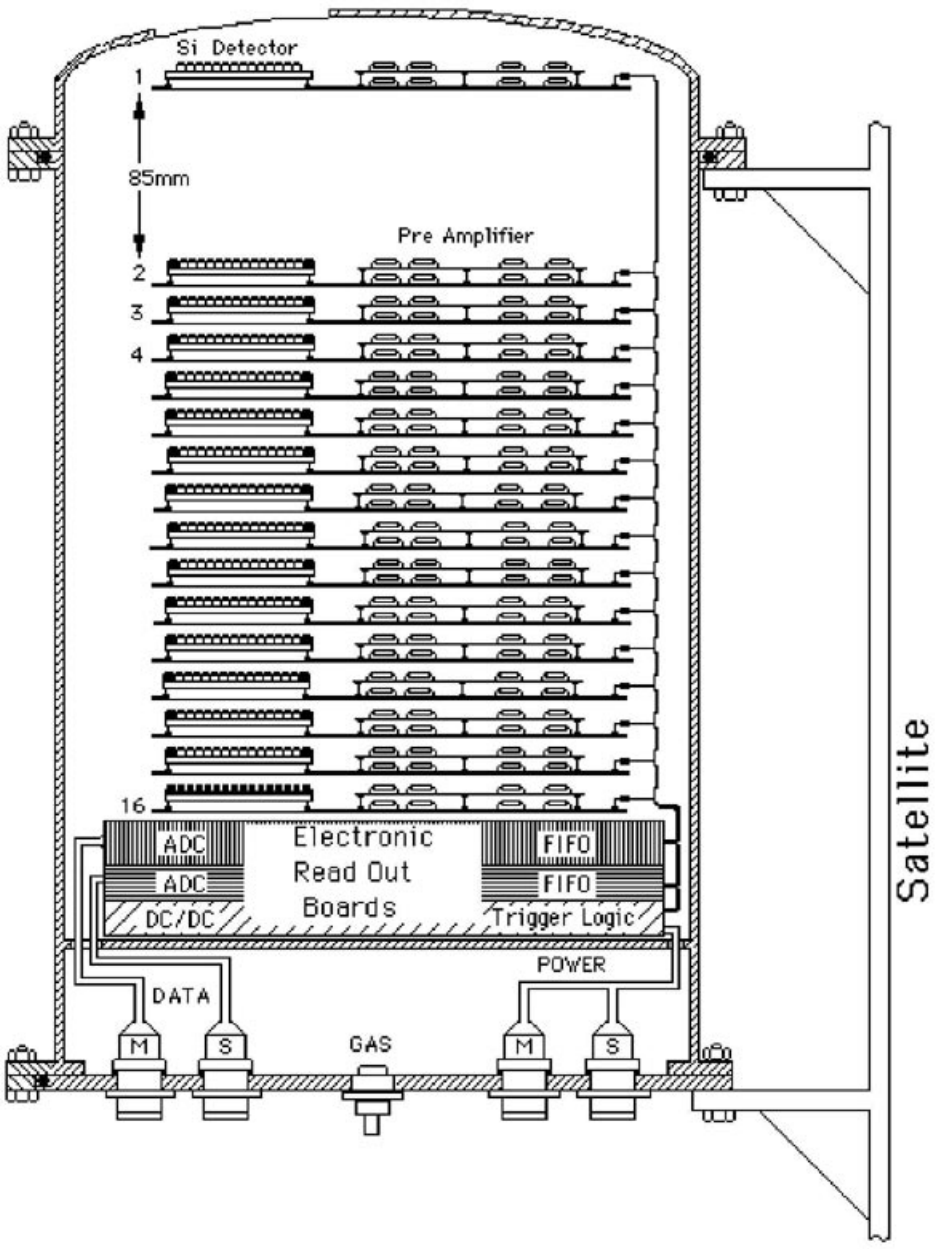

FIG. 2.—Sketch of the internal structure of box *D*1

Laben. Here all tasks of event processing are performed before sending the data to the *interface computer* (box *E*) for mass memory storage.

The core of the box *D*2 are two 8086 microprocessors working with a clock speed of 4 MHz. In normal conditions both of them are operating in master-slave mode: the master microprocessor receives the event from box *D*1 and performs pedestal suppression and data reduction tasks, while the slave is used to format the data, according to the acquisition mode, and send them to the subsystem box *E*. It also selects the trigger logic, implements the second level trigger and interfaces most of the telecommands with the silicon detector.

The *interface computer* (box *E*) represents the last step of the NINA data processing before the records are sent to the satellite for transmission, via telemetry, to ground. Two exemplars of box *E*, for redundancy, have been built, both realized by the Russian company VNIIEM. Finally the *power supply* subsystem (box *P*), made also by VNIIEM, has the function of electrically connecting the satellite with its various subsystems. The primary tension comes from the solar panels, and it is nominally 27 V (between 24 and 34 V). Starting from this, the box *P* provides three different tensions, two for the analog part (+6 V, −6 V) and one for the digital (+5 V), totally independent.

Further details about the instrument and its performance during a test-beam session can be found in Bakaldin et al. (1997) and Bidoli et al. (1999).

3.1. *Operating Modes*

NINA can work in different operating conditions, switched automatically or via telecommand, which affect the trigger system. In particular:

1. Two thresholds for the energy deposited in the single silicon layers have been implemented: a *low threshold* (L.T.),

corresponding to 2.5 mip, and a *high threshold* (H.T.), corresponding to 25 mip.The level of the threshold is fixed by telecommand. As an alternative, a system of automatic switching of the threshold, activated by telecommand, switches automatically from low to high threshold whenever the external rate rises above 10 Hz to prevent the memory being saturated.

2. The strips 1 and 16 of every silicon layer, except the plane first, are used in the lateral anticoincidence system.The hardware lateral anticoincidence can be turned off by telecommand, for instance in case of a malfunction of one of the lateral strips. In this condition, a software veto system (part of the on-line second level trigger) selects only tracks not hitting the lateral strips. This procedure ensures that the lateral anticoincidence rejection is always effective.

3. The planes 15 and 16 can be used as bottom anticoincidence. The default operating mode adopts plane 16, but, in case of need, plane 15 can be selected by telecommand.The bottom anticoincidence can be totally removed by telecommand, allowing the detection of particles crossing the whole apparatus.

The main trigger of the acquisition system is the following:

$$\text{TRG M1} = D_{1x} \times D_{1y} \times [(D_{2x} + D_{2y}) + (D_{3x} + D_{3y})] ,$$

where D_{ij} denotes a signal above-threshold coming from plane i, along view j ($j = x, y$). The logic OR of planes 2 and 3 provides redundancy in case of a failure of plane 2.

In the default operating mode, this trigger is used together with the lateral and bottom anticoincidence ON in order to ensure the complete containment of the particle inside the detector. This is the condition that allows the best energy and nuclear discrimination to be obtained by NINA. Moreover, TRG M1 can be used with low or high threshold, defining two different intervals of nuclei which can be detected. In particular, TRG M1 in high threshold mode removes most of the protons from the trigger. This is the most frequent configuration adopted in orbit.

It is possible to switch, via telecommand, to a second trigger:

$$\text{TRG M2} = (D_{2x} + D_{2y}) \times (D_{3x} + D_{3y}) \times (D_{4x} + D_{4y}) \times (D_{5x} + D_{5y}) ,$$

which is used again in its basic operating mode with the lateral and bottom AC ON. This trigger, used for particular data taking demands or in case of failure of the first plane, increases the acceptance angle, at the expenses of a slight worsening of the angular resolution. The combination of TRG M2 and high threshold again excludes most of the protons from the trigger.

The acceptance window of particles with TRG M1 in full containment regime is shown in Table 1, for low threshold. The spectrum of nuclei extends from hydrogen to iron in the energy interval 10–200 MeV nucleon^{-1}.

The flux of particles changes notably along the orbit. A limit to the acquisition capability of the instrument has been provided by organizing a system which, in high rate conditions, enables the detector to register events in less detail. Every 60 s the processor in box $D2$ calculates the rate of particles reaching the detector, and selects one of the following acquisition modes:

TABLE 1

ENERGY WINDOWS FOR THE MOST ABUNDANT PARTICLES FULLY CONTAINED IN THE DETECTOR NINA, WITH TRG M1 AND ACQUISITION WITH LOW THRESHOLD

Particle	Z	Energy Window (MeV nucleon^{-1})
^{1}H	1	10–48
^{4}He	2	9–50
^{7}Li	3	11–54
^{9}Be	4	13–65
^{11}B	5	15–75
^{12}C	6	17–90
^{14}N	7	18–95
^{16}O	8	20–103
^{19}F	9	21–107
^{20}Ne	10	23–117
^{28}Si	14	28–142
^{40}Ca	20	39–175
^{56}Fe	26	58–195

1. *Full-format mode* (count rate up to 10 Hz).—This mode, in which the whole event topology is recorded, is the normal working configuration outside the Earth's radiation belts and in particular out of the South Atlantic Anomaly (SAA). It allows the measurement of the energy released by the particle in each silicon detector and the storage of this information.

2. E_1-$E_{\rm tot}$ *mode* (count rate $>$ 10 Hz).—At high fluxes it is necessary to make an optimal use of the mass memory. In this acquisition mode, a second level trigger, driven by the processor in $D2$, restricts the event acceptance and calculates the energy E_1 released in the first plane and the energy $E_{\rm tot}$ deposited in the whole detector by the crossing particle. Instead of the whole event topology, only E_1 and $E_{\rm tot}$ are stored.

4. ORBIT OPERATIONS

4.1. *The Satellite Resurs-01*

The class of spacecraft *Resurs-01* is designed for meteorological observations, investigations of Earth natural resources, and large- and small-scale ecological monitoring of the terrestrial environment. Besides these tasks, the spacecraft are also utilized for the separation and insertion into orbit of small piggyback space vehicles.

The *Resurs-01* is inserted into an almost circular Sun-synchronous orbit, having the parameters shown in Table 2. The launch of this class of vehicles takes place from the Baikonur launch facility in Kazakhstan, by means of a Zenit launcher. The total mass of the spacecraft at launch,

TABLE 2

PARAMETERS OF THE *Resurs-01 No. 4* SATELLITE

Characteristic	Value
Orbit inclination (deg)	98.75
Orbit period (minutes)	101.31
Eccentricity	1.12×10^{-3}
Three-axis stabilization accuracy (deg).....	1.0
Average orbit altitude (km)	840

including the separable microsatellites, is 3200 kg. The mass of the payload alone is 1000 kg.

The service system incorporates a power supply (providing a voltage working range from 24 to 34 V), an attitude control and stabilization system (which maintain the attitude of the spacecraft in three axis), a command radio link (designed to control the on-board instrumentation by radio commands), a program-time device (which allows the spacecraft to be in autonomous operation for 3 days), a radiotelemetry system, and an on-board time and frequency standard (which provides stable high-frequency and synchronous signals, and a time mark).

The instrument NINA is housed into *Resurs-01 No. 4* as shown in Figure 3. The box *D*1 is mounted on the top side external to the satellite, in such a way to point always to the zenith during the flight. The other boxes are located inside the body of the satellite.

The box *D*1 has two external sensors to measure its temperature. A heater keeps it thermal stable when switched off. The temperatures of *E* and *P*, and the stability of the satellite power supply, are monitored on board Resurs. All these data are merged with the satellite telemetry and sent to the ground.

4.2. *Control in Orbit*

The interaction between the ground stations and NINA during operations is driven by telecommands, which give the possibility to activate a total of 24 commands. Some are dedicated to operations such as power switching (ON/OFF), data transferring, memory cleaning, and selection of single or dual microprocessor model. The others act on the trigger logic or on the acquisition model, as illustrated previously. The transmission of specific telecommands can be performed when the satellite passes over the ground stations. A response packet with the status of the telecommand settings is sent to Earth each time a change in the command buffer has occurred.

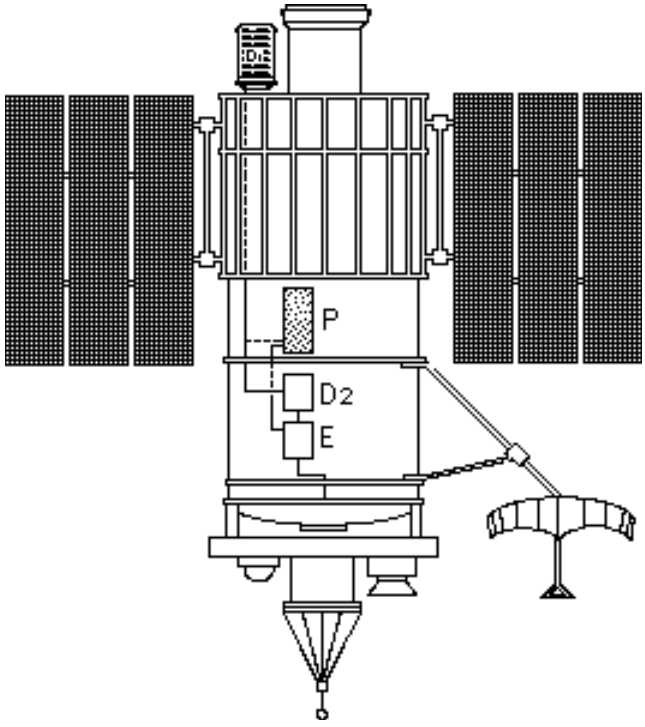

FIG. 3.—Location of the various subsystems of NINA—*D*1, *D*2, *E*, and *P*—on the satellite *Resurs*.

The default telecommand set initializes the acquisition with TRG M1, automatic switching between low and high threshold enabled, lateral strips and bottom plane in anticoincidence, and automatically switching of the acquisition mode from full-format to E_1-$E_{\rm tot}$, according to the count rate. However, it is possible to set any combination of trigger logic, threshold level, anticoincidence, and acquisition mode by telecommand. After 2 months of operation, we switched the acquisition to high threshold mode, in order to focus our analysis on high-Z particles.

A special on-board device allows preprogrammed combinations of telecommands, acting automatically in specific points of the orbit. These combinations permit, for instance, electronic calibration procedures to be performed over the equatorial regions (where the count rate is low) or to stop the data acquisition in sectors of the orbit with very high count rates.

The average volume of data that NINA transfers from the satellite to ground is 2 MB day^{-1}, corresponding to more than 20,000 events. NINA has a 16 MB mass memory available in the on-board memory storage. Since the average mass memory occupation in solar quiet periods and outside the South Atlantic Anomaly is around 1.5 MB day^{-1}, there is the possibility to accumulate data for a few days or during solar events, for a subsequent transmission.

5. DETECTOR PERFORMANCE IN ORBIT

The launch of NINA took place on 1998 July 10. The transmission of its scientific data started on August 31, after an initial period needed for stabilization of the orbit and overall checks of the satellite functionality. The analysis of the first sample of data received showed that the instrument performed well and confirmed the functionality of the whole system.

During one orbit the satellite has a day-night cycle according to its position with respect to the Earth and the Sun. Two of the 34 housekeeping data available on NINA give internal temperatures sampled at two different heights inside the detector. We measured the behavior of the two temperatures in orbit. The excursion of their values between light and shadow was less than 1°, as required in the construction phase.

Important information about the status of the detector is provided by the rate meters, which are also part of the housekeeping sector. These are indicators of the particle flux impinging on different planes of box *D*1, which is a function of the orbit of the satellite. Low- and high-flux rate meters are implemented at different heights inside the telescope. In case of intense flux, the high-rate meters section provides information while the low-rate meters may saturate.

Figure 4 shows the behavior of the low-rate meter implemented on plane 6 during one typical orbit. The count rate is given in hertz, with the saturation value at about 420 Hz. From the picture one can easily follow the path of the satellite through the different regions of the Earth's magnetosphere. In particular, it can be seen how the flux increases at the poles with respect to the equator because at high latitudes the terrestrial magnetic field does not effectively prevent low-energy particles from approaching the Earth. The spikes visible near the poles are due to low-energy

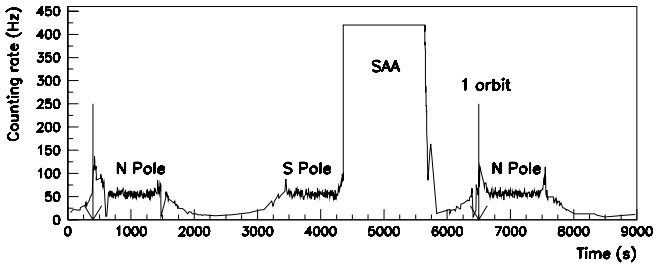

FIG. 4.—Low rate meter count rate (at plane 6) as a function of time. The two black vertical arrows define one satellite orbit.

electrons that fill the outer radiation belt. In the South Atlantic Anomaly the magnetic field has a local minimum, and thus the low-energy proton flux reaches very high levels. This is clearly evident by the saturation of the rate meter counter.

We have examined the stability of some important parameters of the detector with time, during the first 6 months of life of the detector. The pedestal values remained stable within 1 ADC channel from 1998 October until 1999 March. The same holds for the voltages, the threshold values, and the temperatures.

6. GALACTIC COSMIC-RAY MEASUREMENTS

As mentioned before, after the first 2 months of operation, NINA's activity was focused on the detection of particles heavier than hydrogen. In § 6.1 we discuss the track selection algorithm for $Z > 1$ particles that we utilized to calculate the GCR fluxes of ^{4}He, ^{12}C, and ^{16}O, which are shown in § 6.3. The algorithm of isotope identification and the performance of mass discrimination of NINA in orbit are presented in § 6.2.

6.1. *The Track Selection Algorithm*

The optimal performance of NINA in terms of charge, mass, and energy determination is achieved by requesting the full containment of a particle inside the detector, using the lateral and bottom anticoincidence system as a veto. In order to reject upward-moving particles, tracks accompanied by nuclear interactions, and events consisting of two and more tracks, an off-line track selection algorithm for the data analysis is needed.

The selection algorithm for nuclei with $Z > 1$, implemented for the analysis of NINA flight data, applies six rejection criteria:

1. Real particles moving downward and stopping inside the detector have an energy deposition that increases along the track. It is natural, therefore, to request tracks to deposit in each view a quantity of energy greater than in the previous one multiplied by a constant K_1, which takes into account the energy fluctuations. If

$$E(i) < K_1 \times E(i-1) ,$$

for any i in the range from the second crossed view to the one with the maximum deposit of energy, the event is rejected.

2. In order to clean the data sample from particles with nuclear interactions, two energies for each track are calculated:

$E_{\rm track}$ = sum of the energies released by the particle from the first hit view to the view following the one with the maximum deposit of energy.

$E_{\rm residual}$ = total amount of energy left in all the remaining layers.

The two energies are compared and events with

$$E_{\rm residual} > K_2 \times E_{\rm track} ,$$

where K_2 is a parameter to be optimized, are rejected.

3. Double tracks are eliminated estimating two energies for each crossed view i along the particle path:

$E_{\rm cluster}(i)$ = sum of energy released in the strip with the maximum deposit of energy and in the two nearest strips.

$E_{\rm noise}(i)$ = sum of the energy released in the other strips of the silicon layer.

If

$$E_{\rm noise}(i) > K_3 \times E_{\rm cluster}(i) ,$$

for any of the i crossed views and where K_3 has to be fixed, the event is rejected.

4. Events with the maximum deposit of energy in the first view are rejected. This criterion, together with condition 1, selects downward-moving particles.

5. Events in which the maximum energy release in the X view and in the Y view are not in the same or between consecutive detector planes are rejected. This request helps filtering double tracks.

6. In order to reduce the number of particles that leave the detector through the space between planes, events that release the *maximum* of the energy deposit per silicon layer in the strips 2 or 15, for any of the crossed layers, are rejected.

To apply this algorithm to the data collected in orbit it was necessary to choose the K_1, K_2, and K_3 coefficients in such a way to clean the data sample efficiently from the background, minimizing at the same time the number of good events rejected.

In order to optimize these values we utilized samples of different types of particles, obtained from a beam test session at GSI in 1997 (Bidoli et al. 1999), as well as flight data.

If we define as efficiency ϵ the value $\epsilon = [1 - (N.\ \text{rejected good events}/N.\ \text{good events})]$, the best optimization of the K_1, K_2, and K_3 values that we achieved ($K_1 = 0.7$, $K_2 = 0.01$, and $K_3 = 0.01$) determined an efficiency equal to $\epsilon = 0.975 \pm 0.003$ for all particles with $Z > 1$.

6.2. *Isotope Identification*

Charge and mass identification procedures may be applied to the events that survive the track selection algorithm.

The mass M and the charge Z of the particles are calculated in parallel by two methods, in order to have a more precise particle recognition:

1. *The method of the residual range* (Baker et al. 1993; Hasebe et al. 1993; Sparvoli et al. 1997; Bidoli et al. 1999).In this method, the charge Z is estimated by means of the product $E_1 \times E_{\rm tot}$. Here E_1 is the energy released by the particles in the first silicon detector (two layers) of the tower NINA, and $E_{\rm tot}$ is the total energy released in the whole instrument. Figure 5 shows the E_1 versus $E_{\rm tot}$ curves of

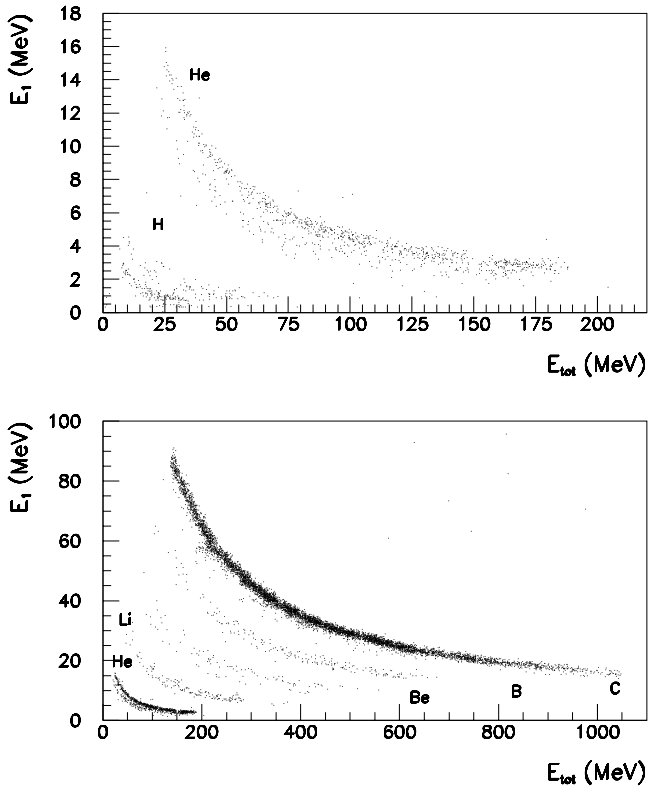

FIG. 5.—Distribution of the energy released in the first plane (E_1) and the total energy (E_{tot}) detected for particles produced in the fragmentation of ^{12}C at GSI.

particles resulting from the fragmentation of ^{12}C by means of a polyethylene target, obtained during a beam test of NINA (Bidoli et al. 1999). The nuclear families lie on different hyperbolas $E_1 \times E_{tot} = k(Z^2)$.Once the charge Z is identified by its $E_1 - E_{tot}$ hyperbole, the mass of the particle is evaluated by applying the following formula:

$$M = \left\{ \frac{a[E_{tot}^b - (E_{tot} - \Delta E)^b]}{Z^2 \Delta x} \right\}^{1/(b-1)} , \quad (1)$$

where ΔE is the energy lost by the particle in a thickness Δx measured starting from the first plane, and the parameter a is a constant depending on the medium and b has a value between 1.5 and 1.8 in NINA's energy range. A precise evaluation of such parameters for each atomic species has been obtained both from real and simulated data.

2. *The method of the approximation to the Bethe-Bloch theoretical curve.*With this second method we estimate the mass M and charge Z of the particle by minimizing the following χ^2 quantity:

$$\chi^2 = \sum_{i=1}^{N} [W_i(\Delta E_i^{real} - \Delta E_i^{theor})]^2 , \quad (2)$$

where ΔE_i^{real} is the energy released by the particle in the ith view, ΔE_i^{theor} is the corresponding expected value, W_i is the weight for every difference $W_i = 1/\Delta E_i^{real}$, and the sum is extended to the N silicon layers activated by the particle, excluding the last one where the particle stops and the fluctuations of the energy deposits are generally very big. In order to build such a function, it is necessary to follow step by step the particle's path, calculating the scattering angles at every layer. This method takes into account also the energy losses in dead layers, thus preventing systematic shifts on the reconstructed masses.

For a complete rejection of the background, only particles with the same final identification given by the two methods are selected. Finally, a cross-check between the real range of the particle in the detector and the expected value according to simulation is a consistency test for the event.

In Figure 6 the reconstructed masses using equation (1) for helium isotopes detected in orbit are compared to the ones obtained from the test-beam data; the sample of particles in orbit has been selected during passages over the polar caps and in periods of quiet solar activity. The figure shows that the mass resolution of NINA in flight is in good agreement with the measurements performed at GSI.

6.3. *Determination of Fluxes*

The analysis presented in this section refers to particles registered by NINA in the solar quiet period 1998 December–1999 March, detected in high threshold mode and TRG M1 acquisition. In order to select a sample of pure low-energy ($E > 10$ MeV nucleon^{-1}) primary cosmic rays and to avoid the distortions induced by the Earth's magnetic field, only particles registered at a value of L-shell > 6 (L geomagnetic shell) were chosen.

In order to estimate the cosmic-ray fluxes, it is also necessary to know the geometric factor of the instrument as a function of energy and the exposure time in orbit. A correction factor can then be applied to account for energy loss in the aluminum window.

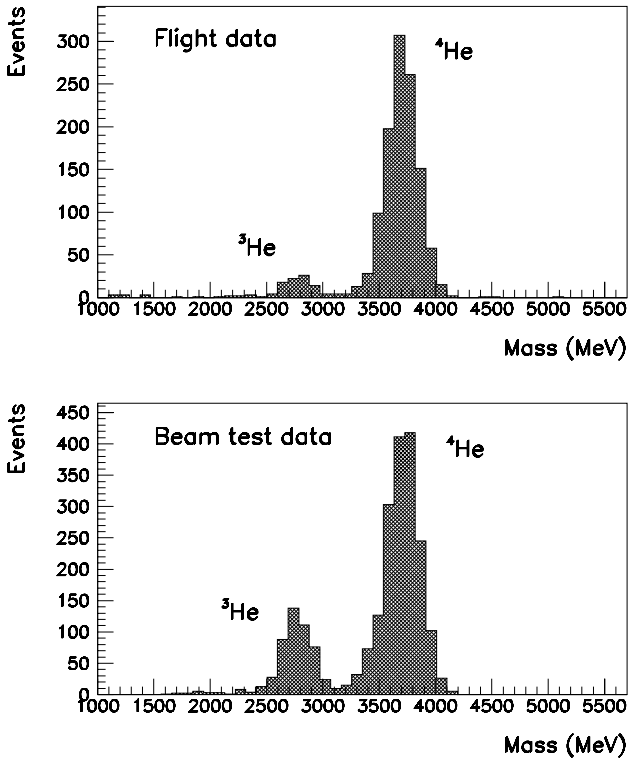

FIG. 6.—Mass distribution, as given by eq. (1), of a sample of helium isotopes collected by NINA in orbit (*top*) and during the beam test session at GSI (*bottom*).

The geometric factor of the instrument was calculated by means of Monte Carlo simulations based on the CERN-GEANT code (Brun et al. 1994). Each simulated track underwent the trigger conditions (TRG M1 or TRG M2), with the lateral and bottom anticoincidences ON, both for low and high threshold mode. Figure 7 presents the geometric factor G of NINA for ^{4}He, ^{12}C, and ^{16}O in high threshold mode over the energy intervals defined by the trigger and the selection conditions explained before.

The incoming energy of the particles was reconstructed by an iterative algorithm, which is based on the Bethe-Bloch formula. The algorithm works this way: as a first step, the total energy $E_{\rm tot}$ is taken as initial energy $E_{\rm in}$ of the particle; with this value of initial energy, all energies deposited in every layer along the particle track (namely the aluminum window, the silicon detectors, and the intergap volumes of nitrogen) are calculated, and the expected value of the total energy deposited in the silicon $E_{\rm tot}^{\rm exp}$ estimated.

The value of $E_{\rm tot}^{\rm exp}$ is then compared with $E_{\rm tot}$. If their difference is greater than 0.1 MeV we define a new initial energy as $E_{\rm in} = E_{\rm tot}^{\rm exp} + E_{\rm step}$, where $E_{\rm step}$ is an incremental step energy fixed according to the precision that we want to reach, and perform a new iteration. When finally the condition

$$E_{\rm tot} - E_{\rm tot}^{\rm exp} \leq 0.1 \text{ MeV}$$

is fulfilled, the algorithm stops and the initial energy of the particle is identified.

The differential energy spectra were then determined by the following formula:

$$\text{Flux}(E) = \frac{\Delta N(E)}{T\epsilon G(E)\Delta E},$$

where $\Delta N(E)$ is the number of detected particles with energy between E and $E + \Delta E$, T is the exposure time in orbit for the period under consideration, ϵ is efficiency of track selection discussed above (0.975 for nuclei with $Z > 1$), $G(E)$ is the average value of the geometrical factor between E and $E + \Delta E$, and ΔE is the energy bin chosen to plot the flux.

Figures 8, 9, and 10 present, respectively, the differential energy spectra for ^{4}He, ^{12}C, and ^{16}O, measured by NINA in the solar quiet period 1998 December–1999 March. Errors due to energy resolution are negligible since the energy resolution for NINA is better than 1 MeV nucleon^{-1}, which is much less than the width of the energy bins in the flux plots.

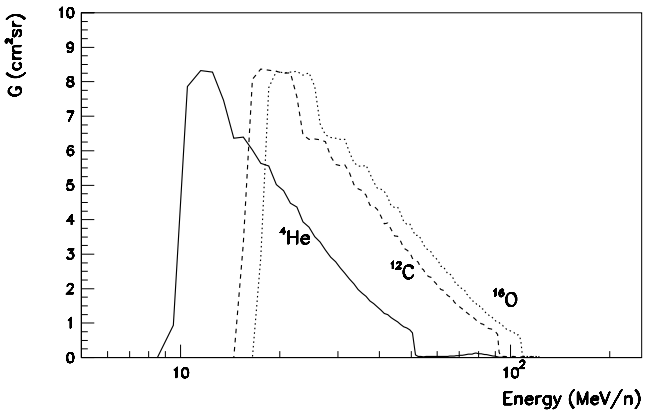

FIG. 7.—Geometric factor G of NINA for ^{4}He, ^{12}C, and ^{16}O in high threshold mode.

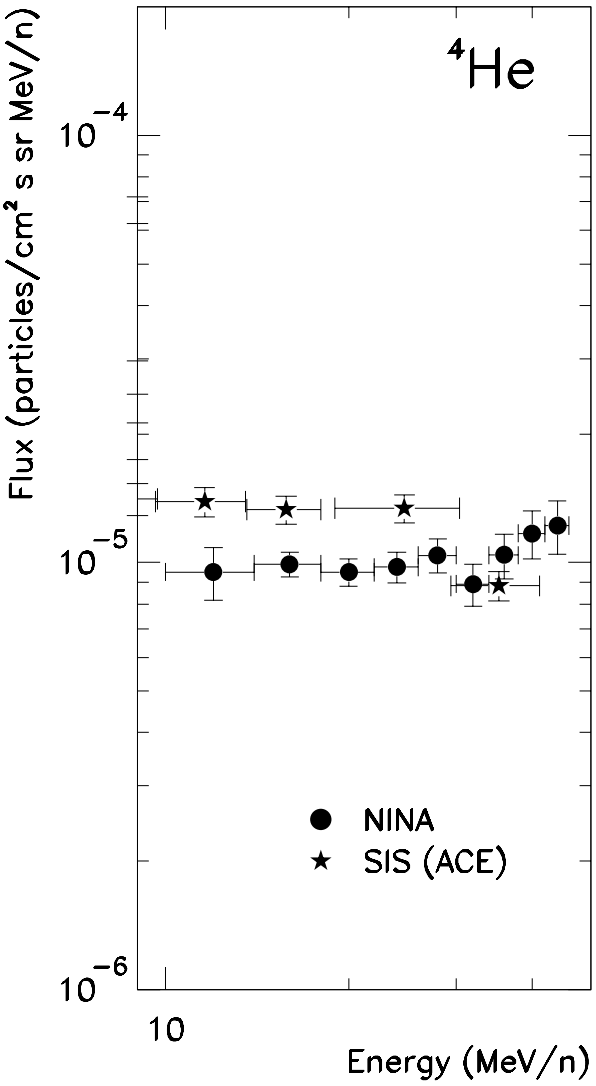

FIG. 8.—Differential energy spectrum for ^{4}He in the solar quiet period 1998 December–1999 March measured by NINA, together with data of SIS on board ACE.

In Figure 8 NINA flux of ^{4}He is plotted together with the results from the mission SIS on ACE, about in the same period of observation. Data from SIS on ACE[2] belong to a cycle of 27 days from 1999 February 6 to 1999 March 4 and are the sum of ^{3}He and ^{4}He; errors are statistic plus systematic.

There is a general agreement among the two sets of results. However, there are differences between the results of NINA and SIS, which can be attributed to the different time period (since the flux of helium is known to change significantly over the months) and to the fact that the SIS flux include also ^{3}He.

In Figures 9 and 10 the NINA differential energy spectra of respectively ^{12}C and ^{16}O are plotted together with results from the missions SIS and CRIS on ACE, both referred to the period 1999 February 6 to 1999 March 4. The fluxes

[2] http://www.srl.caltech.edu/ACE/ASC/level2.

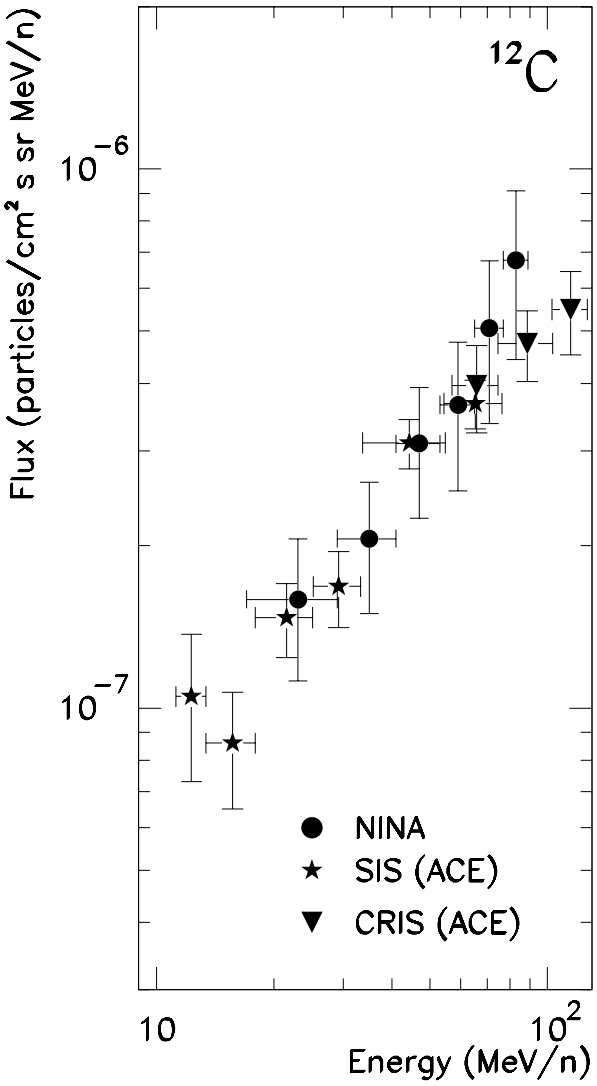

FIG. 9.—Differential energy spectrum for ^{12}C in the solar quiet period December 1998–March 1999 measured by NINA, together with data of SIS and CRIS on board ACE.

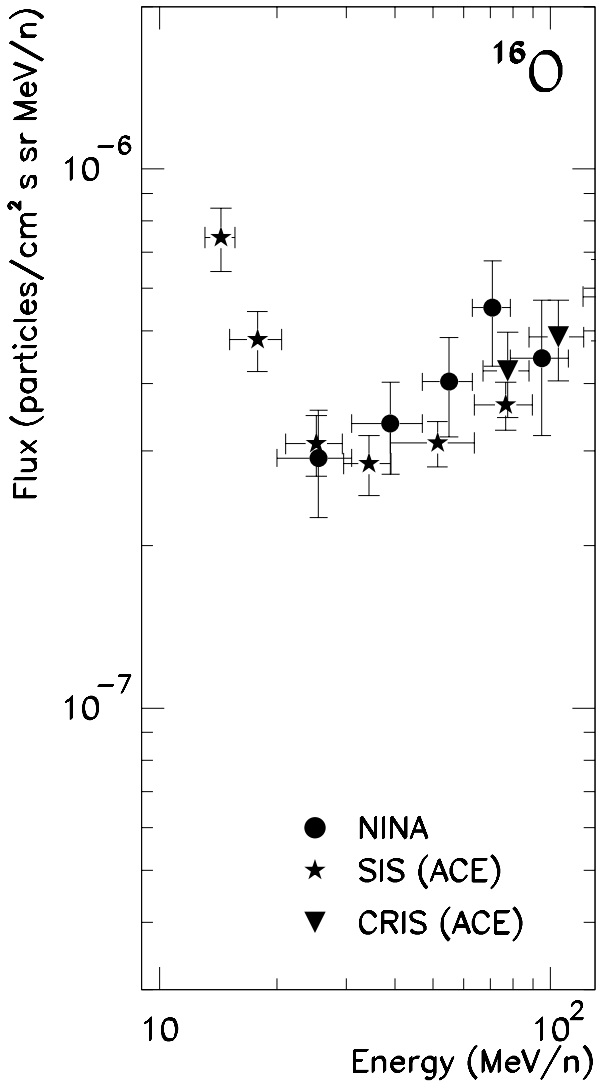

FIG. 10.—Differential energy spectrum for ^{16}O in the solar quiet period 1998 December–1999 March measured by NINA, together with data of SIS and CRIS on board ACE.

measured on board NINA are in very good agreement with the ones on ACE.

7. CONCLUSIONS

The space telescope NINA, launched in 1998, is a silicon detector devoted to the study of cosmic rays of Galactic, solar, and anomalous origin in the energy range 10–200 MeV nucleon^{-1} at 1 AU. It is capable of nuclear identification up to iron and isotopic discrimination up to nitrogen, allowing important space physics issues, such as the composition and energy spectra of cosmic-ray particles, to be addressed.

The first months of data analysis confirmed that the instrument is working properly in space; the overall performances of the detector are in good agreement with expectations, and, in particular, the mass resolution capability reached by NINA in space reproduces the one obtained in a beam test session.

The energy spectra of Galactic ^{4}He, ^{12}C, and ^{16}O measured by NINA at 1 AU have been determined. The analysis of the Galactic ratio ^{3}He/^{4}He together with the abundance ratio of the isotopes of hydrogen is in progress, as well as the study of the composition and energy spectra of SEP and ACR particles.

The measurements performed by NINA are important in view of the second mission NINA-2 which will complement the observations of NINA extending its lifetime to cover a complete solar cycle. The addition of PAMELA (The PAMELA Collaboration 1999; Adriani et al. 1997) will allow the extension of cosmic-ray observations to energies greater than 200 GeV.

We acknowledge the Laben company (Italy) for the realization of *D*1 and *D*2 parts of the detector as well as VNIIEM (Russia) for parts *E*, *P*, and especially for the assembly and space operations on the *Resurs* satellite.

Finally we acknowledge the Russian Foundation of Base Research, grant 99-02-16274, who partially supported the Russian Institutions for this work.

REFERENCES

Adriani, O., et al. 1997, Proc. 25th Int. Cosmic-Ray Conf. (Durban), 5, 49
Bakaldin, A., et al. 1997, Astropart. Phys., 8, 109
Baker, D. N., Mason, G. M., Figueroa, O., Colon, G., Watzin, J. G., & Aleman, R. M. 1993, IEEE Trans. Geosci. Remote Sensing, 31,531
Barbiellini, G., et al. 1996, A&A, 309, L15
Basini, G., et al. 1999, Proc. 26th Int. Cosmic-Ray Conf. (Salt Lake City), 3, 85
Bidoli, V., et al. 1999, Nucl. Instr. Methods Phys. Res. A, 424, 414
Boezio, M., et al. 1997, ApJ, 487, 415
———. 1999, Proc. 26th Int. Cosmic-Ray Conf. (Salt Lake City), 3, 57
———. 2000, ApJ, 532, 653
Brun, R., et al. 1994, Detector Description and Simulation Tool (CERN Program Library)
Casolino, M., et al. 1999a, Proc. 26th Int. Cosmic-Ray Conf. (Salt Lake City), 5, 108
———. 1999b, Proc. 26th Int. Cosmic-Ray Conf. (Salt Lake City), 5, 136
Fisk, L. A., Kozlovsky, B., & Ramaty, R. 1974, ApJ, 190, L35
Golden, R. L., et al. 1994, ApJ, 436, 769
Golden, R. L., et al. 1996, ApJ, 457, L103
Gosling, J. T. 1993, J. Geophys. Res., 98, 18,949
Hasebe, N., et al. 1993, Nucl. Instrum. Methods Phys. Res. A, 325, 335
Hof, M., et al. 1996, ApJ, 467, L33
Klecker, B. 1995, Space Sci. Rev., 72, 419
Klecker, B., et al. 1998, Space Sci. Rev., 83, 259
The PAMELA Collaboration. 1999, Proc. 26th Int. Cosmic-Ray Conf. (Salt Lake City), 5, 96
Pesses, M. E., Jokipii, J. R., & Eichler, D. 1981, ApJ, 246, L85
Reames, D. V. 1990, ApJS, 73, 235
———. 1993, Adv. Space Res., 13, 331
———. 1995, Rev. Geophys. Suppl., 33, 585
———. 1998, Space Sci. Rev., 85, 327
Simpson, J. 1995, Adv. Space Res., 16, 135
Sparvoli, R., et al. 1997, Proc. 25th Int. Cosmic-Ray Conf. (Durban), 2, 181
———. 2000, Nucl. Phys. B, 85, 28
Wiedenbeck, M. E., & Greiner, D. E. 1980, ApJ, 239, L139